AIAA JOURNAL
Vol. 41, No. 10, October 2003

Strain-Rate Effects on Unidirectional Carbon-Fiber Composites

Amit G. Salvi,* Jaeung Chung,† and Anthony M. Waas‡
University of Michigan, Ann Arbor, Michigan 48109-2140
and
Ari Caliskan§
Ford Motor Company, Dearborn, Michigan 48121

Strain-rate effects on mode I fracture of unidirectional carbon-fiber tow composites corresponding to crack propagation parallel to the fiber tow direction was investigated. Precracked unidirectional stitched carbon-fiber specimens were subjected to a static and low-velocity-impact three-point bend test. The crack position as a function of time and hence the crack-propagation velocity were measured with the help of special crack-propagation gauges and a high-resolution digital camera. Load vs load point displacement was measured for every test. The effect of strain rate on fracture energy was characterized. The Iosipescu shear test under static and low-velocity-impact loading conditions was used to characterize the rate-dependent shear response of the material. In addition, tension and compression responses were characterized using American Society for Testing and Materials standard test configurations. It is found that the mode I fracture energy decreases with an increase in the rate of loading.

I. Introduction

TEXTILE fiber composites are an attractive and affordable replacement for pre-preg-based laminated composites in a variety of aerospace and automotive applications. Consequently, several recent studies have focused on manufacturing issues and the deformation response of polymer-based textile fiber composites.[1–4] The ultimate strength and toughness of a composite material are indicators of its ability to absorb energy when subjected to crush loads, either applied slowly (statically) or within a short duration (quasi-statically or dynamically). Because braided and fabric composite structures contain a well-defined microstructure, both the ultimate strength and toughness can be related to microstructural variables. For example, the rate sensitivity of the matrix and the rate sensitivity of the fiber/matrix interface can contribute to the overall rate sensitivity of a composite material at the macroscopic level.

Previous work[5,6] using glass fiber-reinforced braided textile composite tubes have revealed the following important observations with respect to energy absorption. Tests were carried out on [0/±30] braided fabric square cross-section tubes at static and impact velocities in the range of 3–10 m/s. For this range of impact velocity, it was observed that the crush velocity remains fairly constant during the crush process. (This is an assumption. In general, strain gauges placed on the specimen surface during the test shows that strain rate is not constant but changes throughout the loading process.) The constant velocity was achieved by using a high kinetic energy of impact. Under these conditions it has been observed that the tubes fail by delamination and axial cracking as the most dominant modes of failure with substantial fiber/matrix separation occurring in the delaminated fronds. It has also been observed that the crushed tubes always show a larger amount of delamination compared with statically crushed tubes. However, both statically and dynamically crushed tubes show extensive amounts of new fracture surfaces, associated with the failure event. The resin used for the tubes is slightly rate sensitive; however, this indicates that the resin is stiffer and stronger under dynamic conditions. Yet, the dynamically crushed tubes consistently absorb less energy than the statically crushed tubes, always at a lower mean plateau load. Thus, it appears that the rate sensitivity of the fracture events warrant a careful examination.

The basic building block of braided composite plaques are fiber tows that are braided into different microstructural architectures prior to being infused with resin. Different types of braided architectures are summarized in the text.[1] Prior to studying the fracture properties of the braided plaques (the braided plaques contain a complex internal microstructure), it is prudent to understand the various fracture mechanisms and fracture properties of the tows themselves. Fundamental issues related to mode I, mode II, and mixed mode fracture of stitched tow-reinforced composites need investigation. The mode I, mode II, and mixed mode fracture energies are fundamental properties of a fiber-reinforced composite. Consequently, measurement of these fracture energies is necessary for properly characterizing the response and failure of structures made of these composites. In this paper we present the results of an experimental study that examined the mode I fracture of unidirectional carbon-fiber tow composites with crack propagation along the fiber tow direction.

The present investigation of crack growth is limited to low velocity impact (LVI) conditions. Under these conditions the dynamic stress field produced by the impact loading subsides, and this transient field occurs at the very early stages of loading. In the present experiments the maximum impactor velocity is 4.6 m/s, resulting in maximum crack-propagation velocities on the order of 350 m/s. These velocities are a small fraction of the shear wave speed (1540 m/s) and Rayleigh wave speed of the material. Consequently, dynamic effects can be neglected. Researchers[7–11] have conducted an extensive experimental and numerical investigation of dynamic crack propagation in unidirectional continuous fiber (prepreg)-laminated composites. The present study examines continuous fiber (fiber tows) unidirectional composites under LVI conditions.

II. Material Description and Properties

Unidirectional stitched carbon-fiber textile composites were used for this study. Fibers are stitched together in bundles to form fiber tows. Approximately 80,000 fibers were bundled in one tow. These fiber tows were then stitched together to form a unidirectional fiber mat. Ten such fiber mats were stacked one on top of another, and vinyl ester resin is infused into a mold containing the stacked mats. After the matrix is infused and because of the consolidation pressure

Received 21 October 2002; revision received 1 May 2003; accepted for publication 20 May 2003.

*Graduate Student Research Assistant, Department of Aerospace Engineering, Composite Structures Laboratory.
†Postdoctoral Fellow, Department of Aerospace Engineering, Composite Structures Laboratory.
‡Professor, Department of Aerospace Engineering, Composite Structures Laboratory. Associate Fellow AIAA.
§Research Engineer, Safety R and D Department, 2101 Village Road.

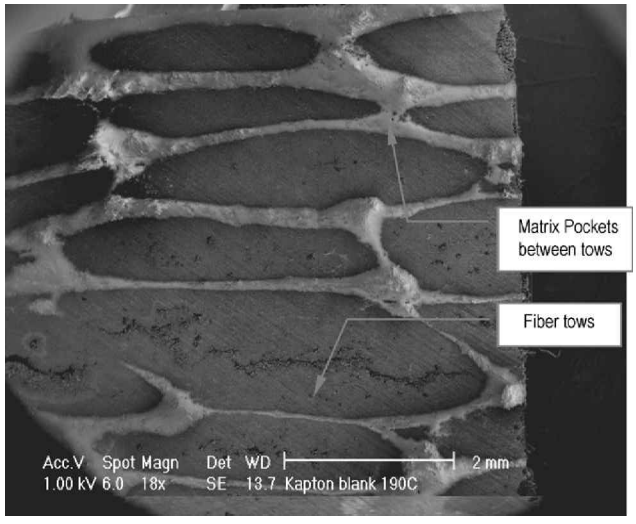

Fig. 1 Cross sections of the specimen.

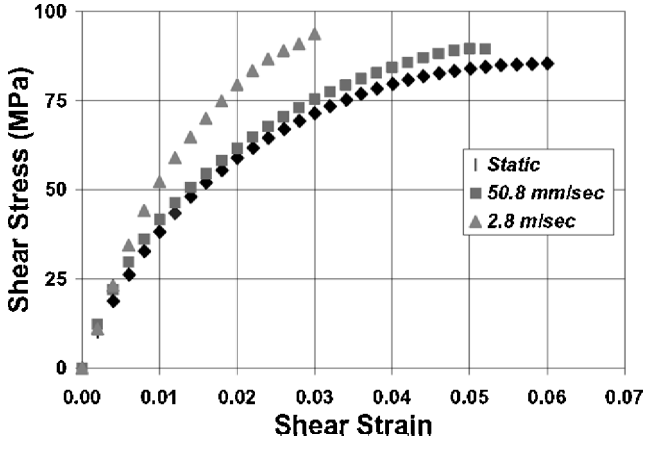

Fig. 2a Shear stress vs shear strain behavior (case: 90 deg).

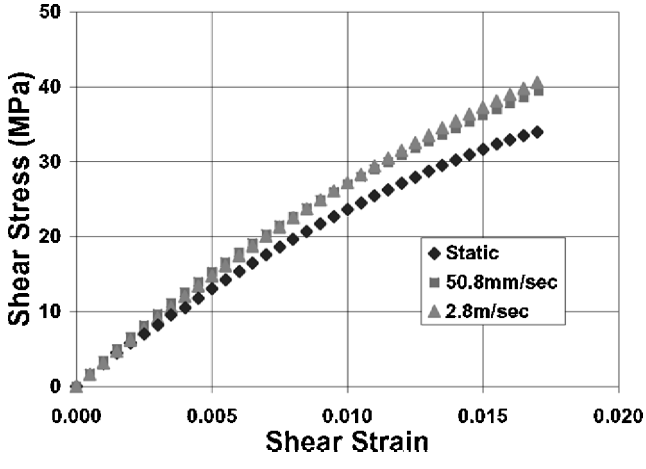

Fig. 2b Shear stress vs shear strain behavior (case: 0 deg).

exerted by the mold, the cross section of the fiber tows becomes oval in shape. This gives the resulting material a unique microstructure as shown in Fig. 1. The thickness of the specimens is approximately 7.62 mm.

Iosipescu shear specimens, 76.2×25.4 mm long with a 12.7-mm-wide notch in the center, were cut. Test specimens were cut at fiber angles of 0 and 90 deg with respect to the direction of loading. The shear response was obtained under static and LVI conditions. From these tests the shear response of the material was obtained as function of loading rate. Similarly, the compression properties of

Table 1 Shear modulus under static and quasi-static loading

Test impactor velocity	Shear modulus (zero), GPa	Shear modulus (90), GPa
Static	2.89	4.30
50.8 mm/s	3.19	4.97
2.8 m/s	3.32	5.74

Table 2 Material properties of the specimen under static and LVI condition

Test	E_{11}, GPa	E_{22}, GPa	G_{12}, GPa	ν_{12}
Static	79.3	8.27	1.17	0.24
LVI (2.8 m/s)	79.3	8.27	1.55	0.24

the plaques in the principal orthotropic directions were measured. These were found to be rate insensitive in the regime of loading rates examined (0–5 m/s, under LVI conditions).

The low rate Iosipescu shear tests[12] were carried out with an actuator velocity of 50.80 mm/s on a Materials Test Systems (MTS) loading frame, whereas the LVI tests were carried out on a drop tower. A dead mass of approximately 43 kg was dropped on the moving grip of the Iosipescu shear fixture. Load was measured via a load cell placed in the impactor of the drop tower. The shear response measured from the Iosipescu tests are shown in Figs. 2a and 2b. Figure 2a shows the shear response of the 90-deg specimen configuration. Figure 2b shows the shear response of the 0-deg specimen configuration. The values of the shear modulus G_{12} obtained from these plots are shown in Table 1. Table 2 shows the other elastic properties, including the major Poissons ratio.

III. Three-Point Bend (Fracture) Tests

The test specimens of size 63.50×88.90 mm (2.5×3.5 in.) were cut such that the fiber tows lie in the direction of loading. A centrally placed end notch 1 mm wide and 12.70 mm in depth was introduced. A sharp knife edge was used to make the crack tip fine.

Specimens were loaded in a three-point bend configuration with the help of three steel rollers of diameter 12.70 mm (0.50 in.). The top roller was placed along the line of the crack. Bottom rollers were placed at 76.2 mm apart, and the specimen was centered on these rollers. One side of the specimen was painted with reflective silver paint to photograph the crack propagation. A special crack-propagation gauge was placed on the other side to detect crack growth during the static and LVI tests.

Static fracture tests were carried out on a hydraulically activated MTS loading machine. Load was introduced through the top-loading pin at the rate of 0.01016 mm/s. Load P and load point displacement Δ between loading pins were recorded. Simultaneously, a high-resolution Kodak digital camera (2028×2044 pixels) was programmed to capture pictures of the propagating crack at 1-s intervals. The camera was focused around the notch area to give the exact location of the crack tip. Thus the extension of the crack was measured at 1-s increments during the loading of the specimen. The loading was terminated when the crack reached the vicinity of the top roller.

LVI tests were carried out on a drop tower facility. The test configuration was similar to the static tests. A drop weight of approximately 43 kg was dropped on the top loading pin from heights of 40 cm (impactor velocity: 2.8 m/s) and 108 cm (impactor velocity: 4.6 m/s). The load experienced by the specimen was measured by a Kistler impact load cell, which was attached to the impactor. The force signal was then used to calculate the acceleration of the top loading pin (by dividing the force signal by the mass of the impactor). This acceleration was integrated once to get the velocity of the loading pin and twice to get the position of the loading pin. It is assumed that the deformation of the impactor is negligible while computing the load point displacement. The movement of the loading pin was found to be uniform, which implies that sufficient energy was provided by the impactor to maintain a constant displacement

rate of loading. The recorded load and load point displacement were plotted against each other for all of the LVI tests.

A crack-propagation gauge (Vishay special purpose strain gauge CPC03), connected across a simple electrical circuit, was used to detect the crack position during the LVI test. The gauge consists of a pattern of parallel lines made of conducting material. When each line of the gauge is severed, the total resistance of the gauge is altered. By measuring the change in the resistance of the gauge, the location of the crack tip can be found to within the spacing of the lines in the gauge. The gauge used has 20 grid lines that are spaced 2 mm apart. This gauge was placed in the intended path of the crack. As the crack propagates, the conductive lines in its path are severed, thus altering the electrical resistance across it. A high-speed data-acquisition (2-GHz) oscilloscope in conjunction with a Wheatstone bridge circuit was used to record the change in the resistance. A calibration curve of distance vs the resistance was used to calculate the position of the crack as a function of time.

A high-speed digital camera (CORDIN 220, capable of taking pictures at every 100 ns) was also used to capture images of crack propagation during loading. This camera was triggered as soon as the impactor hits the specimen, and eight subsequent pictures were taken at prespecified time intervals. The images were analyzed to cross check the data obtained from the crack-propagation gauge.

IV. Experimental Observations

A. Static Fracture Tests

Load vs load point displacement data are shown in Fig. 3a. The point at which the initial crack starts to grow is also indicated. When the load point displacement Δ reaches approximately 1.20 mm, the crack tip has reached the vicinity of the load point roller. Thus,

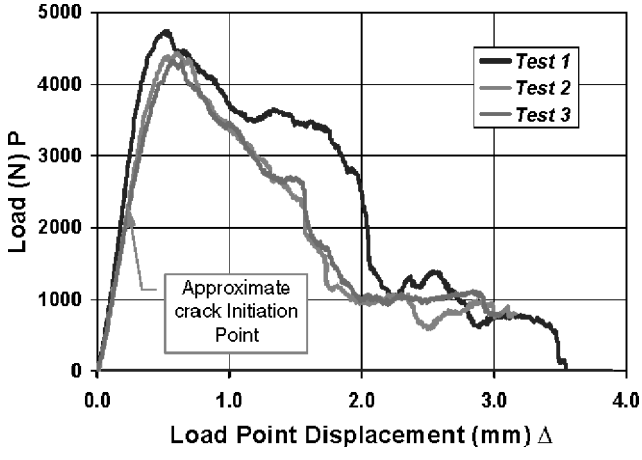

Fig. 3a Load vs load point displacement (static case).

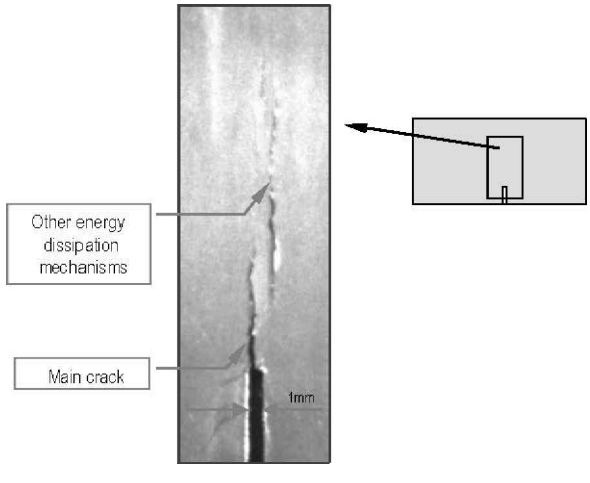

Fig. 3b Crack growth captured by high-resolution camera.

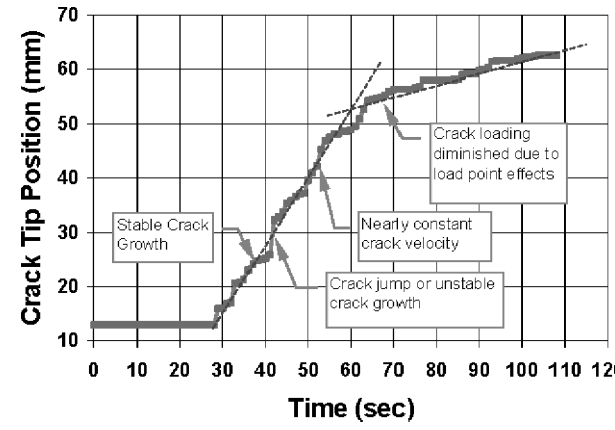

Fig. 3c Crack initiation and progression in the specimen.

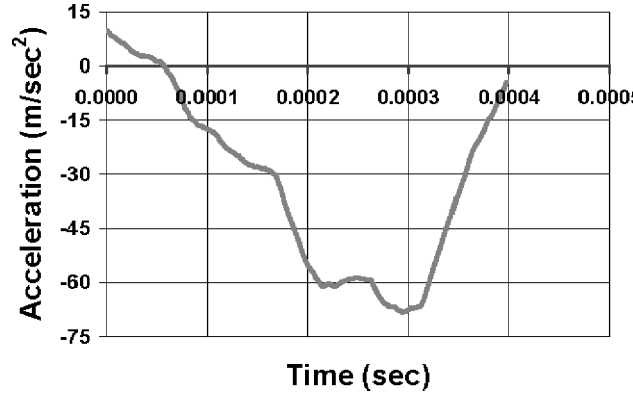

Fig. 4a Impactor acceleration, velocity and displacement.

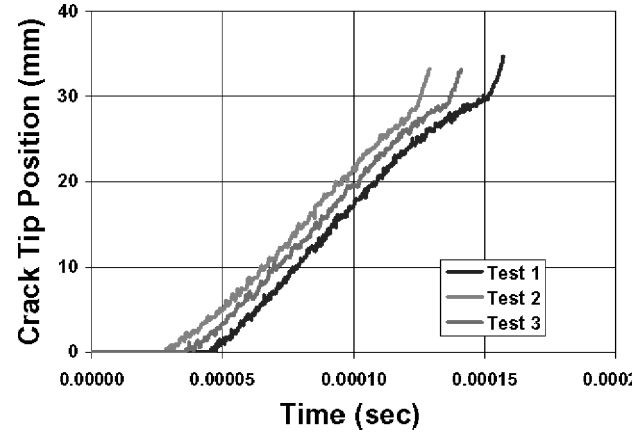

Fig. 4b Typical signal from special crack-propagation gauge.

beyond this Δ the data are a measure of the crack propagation into material that has been crushed by the load point roller. We shall not consider the data beyond $\Delta = 1.20$ mm any further. Figure 3b shows the photographed area of the notch during crack propagation. While the primary crack is growing, secondary crack formation, as shown in Fig. 3b, is noted. Postexperiment micrographs from regions adjacent to the primary crack indicated substantial secondary cracking caused by static loading. This is discussed in detail in later sections. It is clear that the primary crack propagation is not smooth, indicating durations of no crack growth and spurts of crack growth occurring almost instantaneously. On average, we can identify two regions of almost constant velocity crack growth as shown in Fig. 3c.

B. Low-Velocity-Impact Fracture Tests

Figure 4a shows the acceleration of the impactor under static and LVI conditions. This acceleration is integrated twice to get the

displacement of the load point. Figure 4b shows a typical signal from the special crack-propagation gauge for LVI tests. This crack-propagation gauge provides an accurate and consistent measure of the crack location during LVI tests. Figure 4c shows a typical load vs load point displacement behavior for a LVI test carried out at an impactor velocity of 2.8 m/s. Low-velocity tests were observed to be very sensitive to the notch position along the microstructure of the specimen (whether the initial notch is placed between two tows or through a single fiber tow). Pictures taken with the help of the high-speed camera are shown in Fig. 4d. The position of the crack visually measured from these images is found to be consistent with the readings obtained from the crack-propagation gauge.

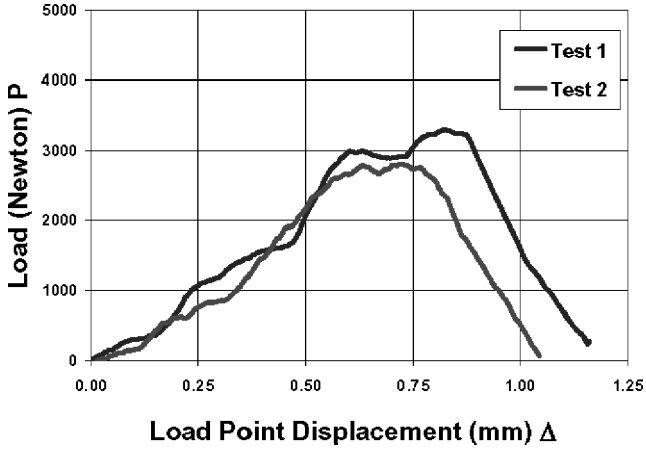

Fig. 4c Load vs load point displacement behavior (quasi-static), 2.8 m/s.

C. Energy Absorption Under Static and Low-Velocity-Impact Conditions

Figure 5 shows the comparison between the load vs the load point displacement behavior for static and LVI tests. The maximum loads for the LVI tests were observed to be consistently lower than that of the static test. The area under the curve is approximately a measure of the energy absorbed during the loading duration. Consequently, it was seen that in these specimens, under mode I fracture conditions, the energy absorption was greater for static fracture when compared against the LVI cases.

Higher static load (and fracture energy) can be attributed to rate-dependent inelastic mechanisms that are at work during crack propagation. Under static conditions the specimen was observed to have a considerable amount of fiber bridging associated with primary crack propagation (even though the specimen is unidirectional). In addition, secondary cracking was also visible. As a result, the primary crack path is not well defined. Even though a crack has propagated in the material, it was not failed completely. Under LVI conditions the crack interface was much smoother compared to the static case. Fiber bridging was observed to be very small or almost absent. This results in the rapid drop of load accompanying crack growth.

The measurements indicate that crack growth under LVI conditions occurs much faster (time to initiation is much shorter)

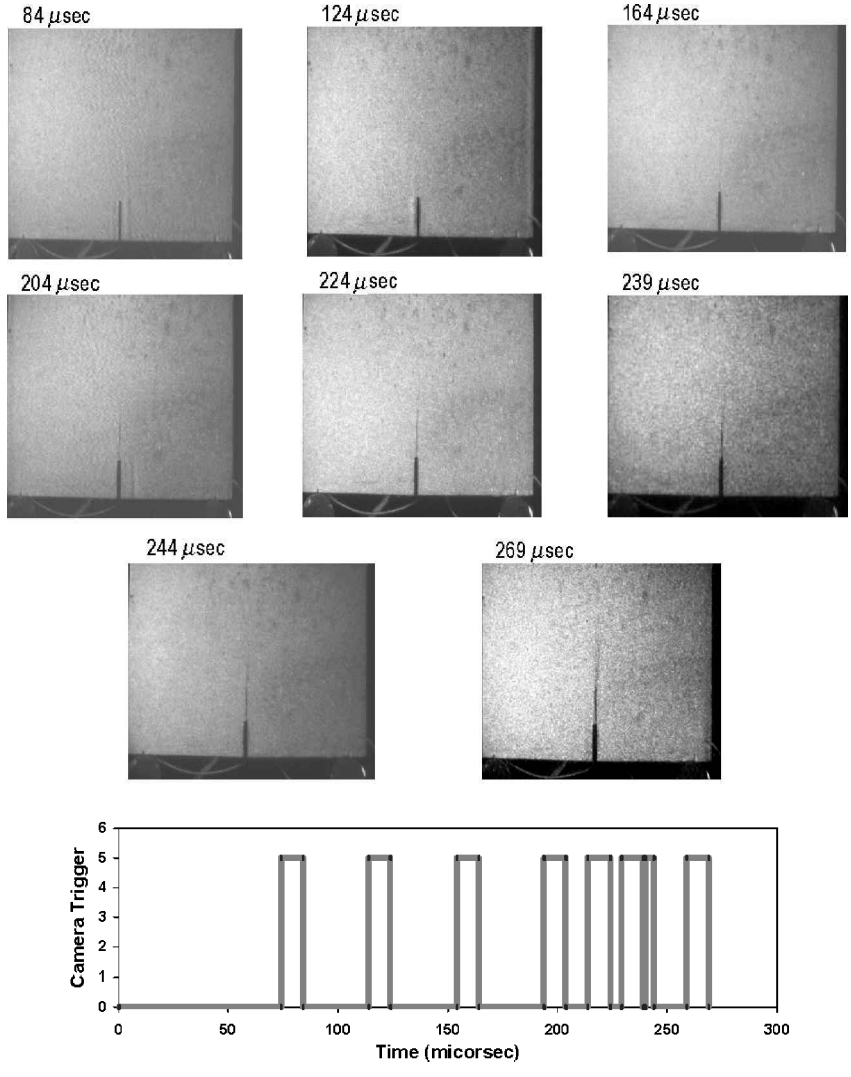

Fig. 4d Crack growth captured by high-speed camera.

Table 3 Values of load and load point displacement at crack initiation point

Static test		2.8 m/s		4.6 m/s	
Load point displacement, mm	Load, N	Load point displacement, mm	Load, N	Load point displacement, mm	Load, N
0.28	2813	0.19	591	0.13	307
0.34	2609	0.15	560	0.16	302

Table 4 Values of compressive strains measured away from the crack path

Test	Far-field strains (microstrains)
Static	1200.00
2.8 m/s	432.00
4.6 m/s	163.00

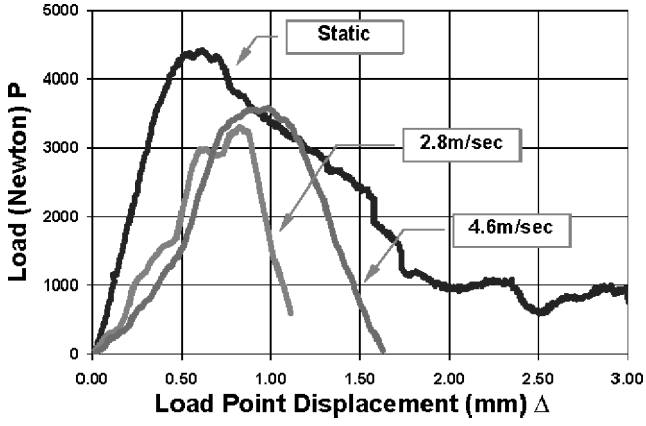

Fig. 5 Comparison (P vs Δ) between static and quasi-static tests.

compared to the static case. Consequently, the volume of material that is subjected to intense loading because of the presence of the crack is much smaller for the LVI case compared to the static case. The stored strain energy is more focused and localized around the crack tip region. The next section of this paper provides additional evidence to substantiate these claims. The size of the damage zone in front of the notch during static crack initiation and growth was found to be much larger than that corresponding to the LVI case. The trend in the data shows that the size of the damage zone associated with crack propagation decreases as the crack velocity (or the rate of loading) increases. This is further discussed in the next section.

V. Discussion of Results

A. Crack Initiation Point

For the fracture tests (static as well as LVI) the load reading at the point of crack initiation was noted, that is, the load at which the first crack growth appears. Table 3 lists the load and load point displacement corresponding to crack initiation. For static tests the crack initiates after a sufficiently long time after initiation of loading. Because of this long time period, different regions of the specimen reach equilibrium at the same time prior to crack initiation, that is the stored strain energy is more diffused. Under LVI conditions, because of the relatively short time interval between load initiation and crack growth initiation, different regions of the specimen are subjected to vastly different stress and strain states. Consequently, the deformation zone is more localized. A smaller volume of material around the crack tip is subjected to intense stress and strain rate. To further strengthen these observations, strain gauges were placed away from the intended crack path as shown in Fig. 6a. The value of strain recorded by this gauge was noted under static and LVI conditions. The maximum compressive strain in the specimen under static and low-velocity-impact conditions as indicated by this gauge are given in Table 4.

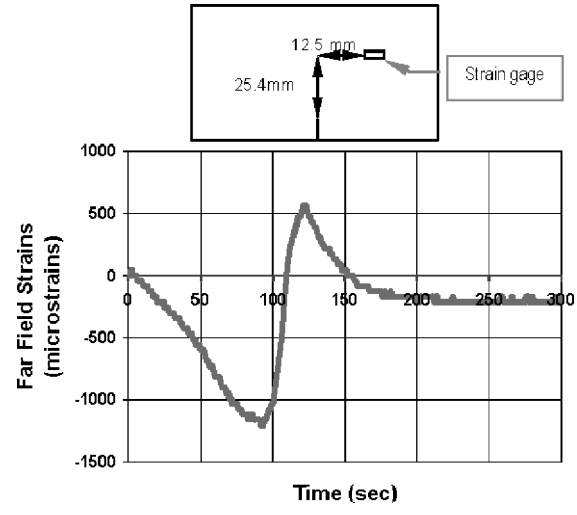

Fig. 6a Strains collected away from the notch.

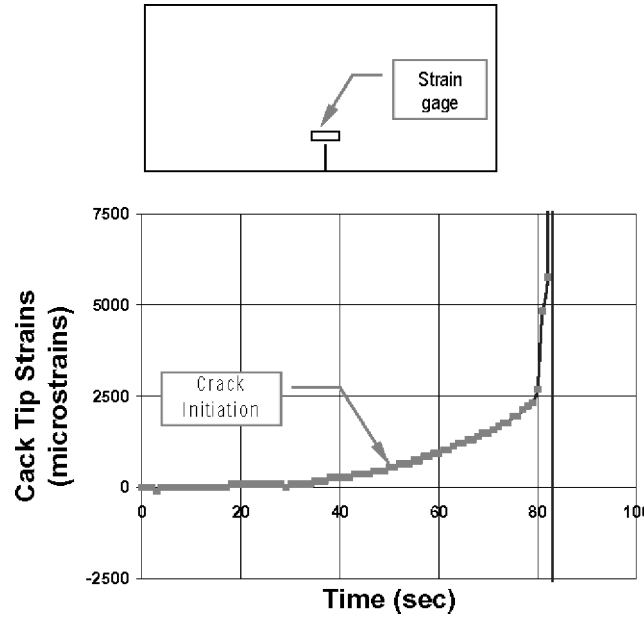

Fig. 6b Strains collected near the crack tip.

Under LVI conditions, because deformation energy is highly localized, a critical condition corresponding to a lower external load and external displacement is reached sooner. Thus, crack initiation occurs at a lower external load. Whereas under static conditions, the deformation energy is more diffused, leading to the triggering of other energy absorption mechanisms, for example, secondary cracks.

B. Load Point Displacement and Crack Tip Strains

When load point displacement Δ for static and LVI tests were compared, it was seen that for a given load Δ is much larger in the low-velocity-impact case than the static case. Further, Δ scales with the rate of loading, being largest for the case corresponding to an

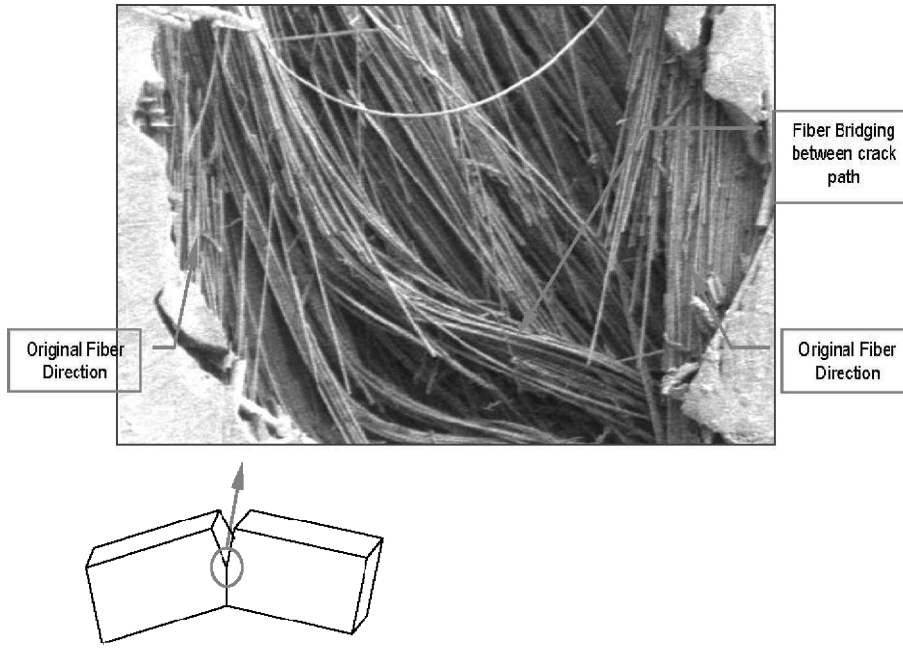

Fig. 7a Fiber bridging observed under microscope.

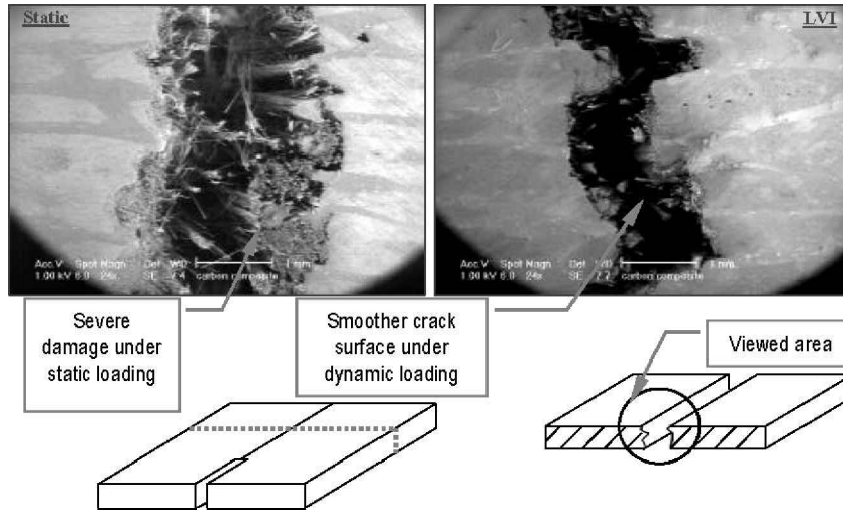

Fig. 7b Cross section of crack zone observed in the crack path.

Table 5 Values of tensile strains measured 1 mm away from notch tip

Test	Notch tip strains (microstrains)
Static	744.00
2.8 m/s	4190.00
4.6 m/s	118857.00

impactor velocity of 4.6 m/s. For the same external load state the amount by which the crack has grown was largest for the case of impactor velocity 4.6 m/s and smallest for the static case. Consequently, the load point displacement was largest for the case corresponding to an impactor velocity of 4.6 m/s.

A strain gauge was placed very near the crack tip on the specimen perpendicular to the intended crack path and ahead of the crack tip. The center of the gauge was located at a distance 2 mm ahead of the crack tip. A typical strain vs time plot is shown in Fig. 6b. Crack tip strain values corresponding to the crack initiation point (measured for each test) are shown in Table 5.

The value of strain under LVI conditions was very high compared to the static case. This substantiates the highly intense local deformation under LVI conditions.

C. Crack Path Interface

For static tests extreme fiber bridging of the crack path was observed. Fibers were pulled out away from the actual crack path forming a large damage (or process) zone. Cracked specimens were observed under a scanning electron microscope to investigate the damage.

Figure 7a shows fiber bridging observed under an optical microscope. Figure 7b shows a comparison between static and a LVI test specimen after fracture. Specimens were sectioned as shown in the figure. When the crack interface was viewed, it is seen that the crack surface is much smoother under LVI conditions. Figure 7c shows a comparison between static and LVI damage zones. As is clearly indicated in these images, extensive fiber/matrix separations accompany the primary crack propagation in the static case, whereas dynamic crack growth occurs with very little energy dissipation occurring elsewhere (other than the primary crack path). To compute the fracture energy associated with primary crack propagation, the

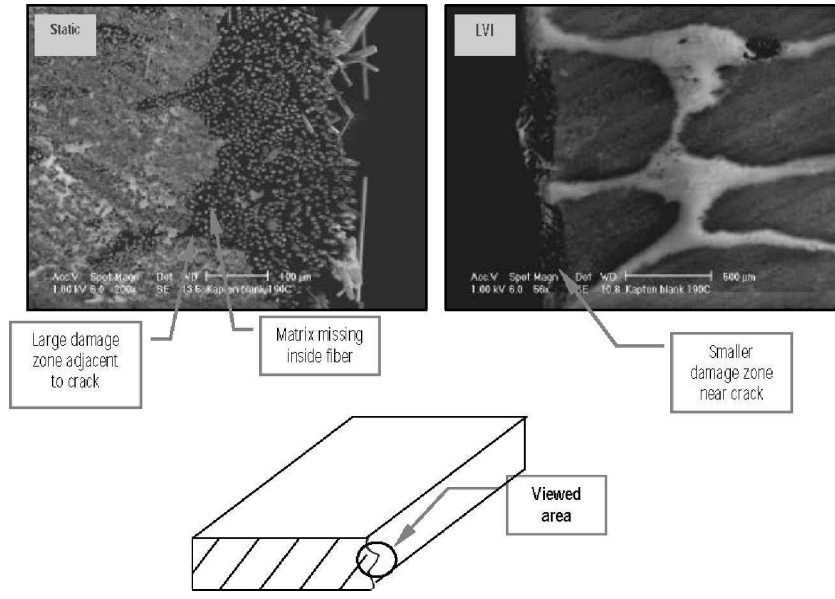

Fig. 7c Damage zone near crack interface.

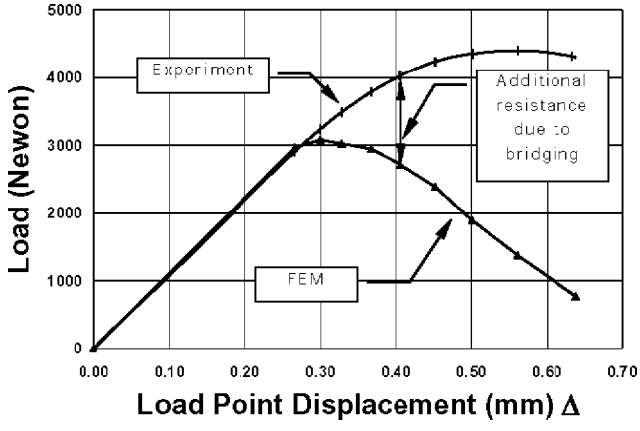

Fig. 8a Load vs load point displacement (static case).

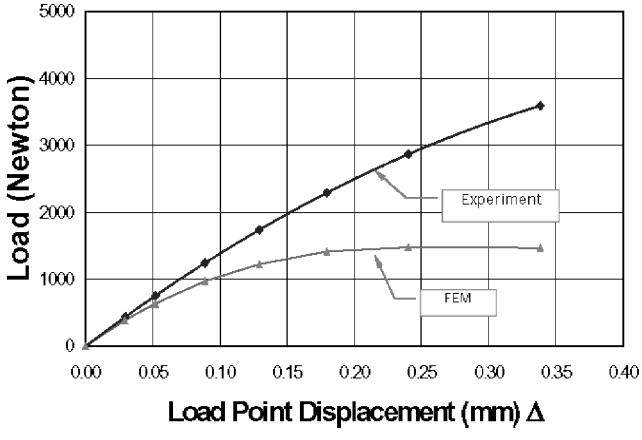

Fig. 8b Load vs load point displacement (quasi-static case: 2.8 m/s).

experimental results were analyzed in conjunction with a finite element model of the test configuration. The computational work is explained next.

VI. Computational Model

A computational model was implemented using the commercial finite element (FE) software package Abaqus. The initial slope of the load vs load point displacement curve predicted by the FE analysis was matched to the experimentally measured data by using an

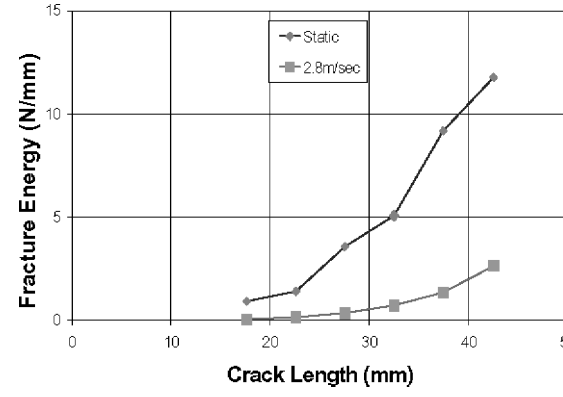

Fig. 8c Comparison between fracture toughness (static and quasi-static case).

adjusted value of shear modulus G_{12}. Such an adjustment of G_{12} was favored over a very detailed model of localized deformation under the roller supports. The roller support loading and the center roller loading were modeled as point loads. Subsequently, an FE analysis incorporating geometric nonlinearity was conducted. Crack length was varied and the equilibrium load P vs load point displacement Δ curve was generated. Results obtained from such analyses are shown in Fig. 8a (static) and Fig. 8b (low velocity impact). On these plots the experimental load vs load point displacement measurements are also indicated. The material properties used in the FE analysis are given in Table 2.

For a given crack length the FE analysis enables us to calculate the recoverable elastic energy stored in the specimen, whereas the experimental measurements provide the total energy absorbed at that same state. The difference between these two energies supplies the unrecoverable energy associated with crack growth. The fracture energy is plotted against crack length in Fig. 8c for the static case and for the LVI case corresponding to an impactor velocity of 2.8 m/s. As the crack grows, more resistance is encountered as a result of fiber bridging, with the bridging resistance increasing with the crack length. This rate of increase of fiber-bridging toughness was larger for the static case when compared to the LVI case. This shows that static fracture leads to a larger damage zone ahead of the propagating crack (diffused damage), whereas LVI crack propagation leads to a localized damage zone with the size of the damage zone scaling inversely with crack velocity. This implies that in the limit of exceedingly large crack tip velocities all of the external work input is transmitted uninterrupted to the crack for the creation

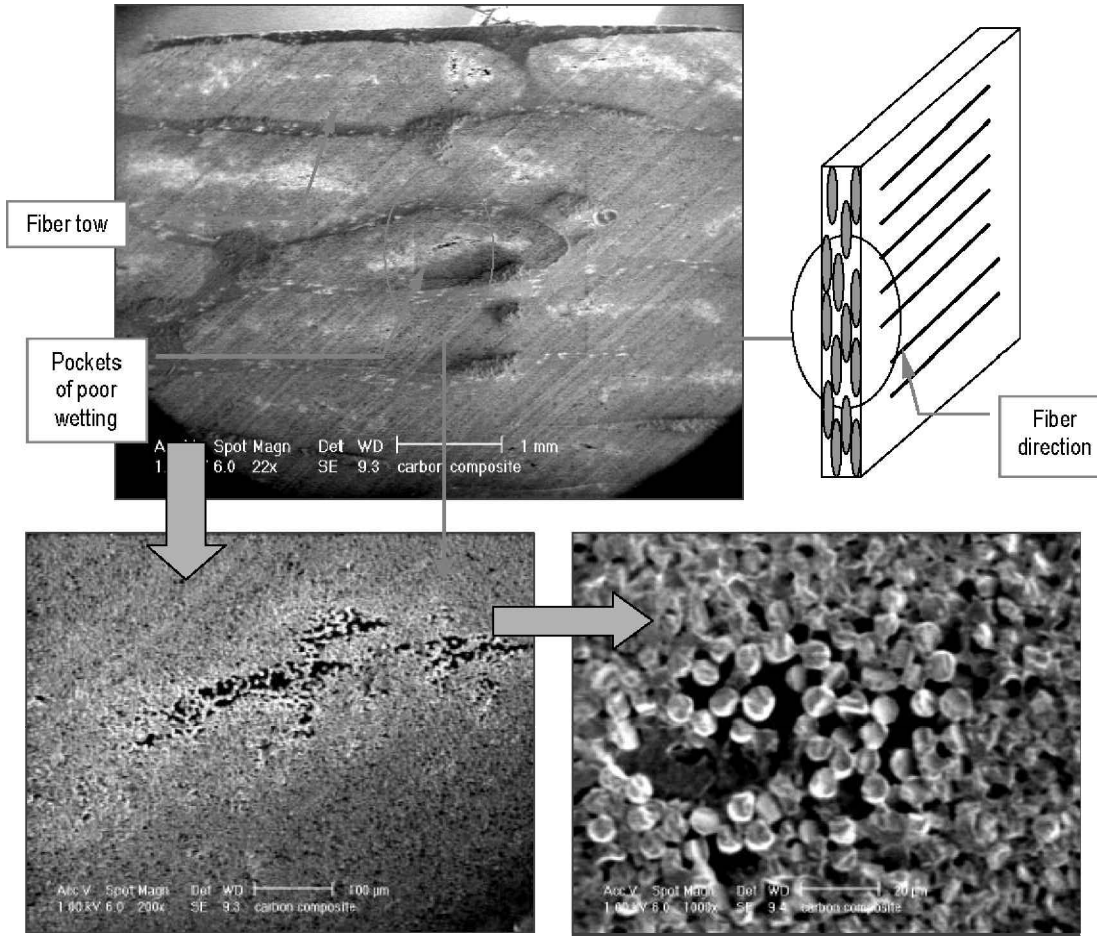

Fig. 9 Imperfections inside fiber tows in the specimen.

of a clean fracture surface. Of course, these comments are applicable to very sharp cracks and to the present textile composite specimens. Clearly, there exists a "competition" between the dynamic mode I crack initiation energy (Ref. 9 within the context of the present discussion) and the mode I fracture energy.

VII. Material Imperfections

When specimens are observed under a scanning electron microscope as shown in Fig. 9, material imperfections caused by the manufacturing process are found to be present. Poor fiber wetting and thus unintended voids within a fiber tow are observed. Under LVI conditions specimens are more sensitive to these imperfections compared to static conditions.

As the remote loading rate increases, the stress intensity at the crack tip is found to be severe and more localized. At the same time the resistance to fracture, caused by these unintended imperfections, decreases as a function of loading rate. Thus, two detrimental events occur as the rate of loading increases. On the one hand, the severity of the localized stress field builds up more quickly (the stresses at the crack tip rise much faster), and at the same time the resistance to fracture (a rate-dependent local material property) decreases. The overall result is early fracture and thus reduced energy absorption. In mathematical terms, for a mode I crack, fracture occurs when

$$K_I(\dot{\varepsilon}_l) = K_{Ic}(\dot{\varepsilon}_l)$$

where the left-hand side of the preceding equation shows the stress intensity at the crack tip (a function of local strain rate) and the right-hand side is a material property (the resistance of the material to fracture, which is a function of the local loading rate). As just explained, with increasing remote loading rate the left-hand side builds up more quickly and at the same time (because of microstructural flaws) the right-hand side decreases. Thus, reduced energy absorption at higher rates is measured in the experimental investigation.

VIII. Conclusions

The mode I fracture energy of fiber tow-reinforced unidirectional carbon-fiber composites have been characterized via a combination of experiment and finite element analysis. Both the elastic shear modulus and the inelastic shear response show a rate dependency. These properties exhibit "hardening" behavior. The mode I fracture energy shows a reversed trend with the rate of loading. It is found that the fracture energy decreases with an increase in the rate of loading. The reasons for this behavior are explained by appealing to the composite microstructure and the observed failure mechanisms.

Acknowledgments

The authors thank the U.S. Department of Energy program management team and the board and staff of the Automotive Composites Consortium. This work was sponsored by the Automotive Composites Consortium and the U. S. Department of Energy, Office of Transportation Technologies, Office of Advance Automotive Technologies, Lightweight Materials Program, under Cooperative Agreement Number DE-FC05-95OR22363. A. Salvi and A. M. Waas thank the aerospace engineering department at the University of Michigan.

References

[1] Chou, T. W., "Microstructural Design of Fiber Composites," *Cambridge Solid State Science Series*, 1992.

[2] Miravette, A., *3-D Textile Reinforcements in Composite Materials, Woodhead Publishing Limited*, CRC Press, 1999.

[3] Adeyemi, N. B., Shivakumar, K. N., and Avva, V. S., "Delamination Fracture Toughness of Woven-Fabric Composites Under Mixed-Mode Loading," *AIAA Journal*, Vol. 37, No. 4, 1999, pp. 517–520.

[4]Shivakumar, K. N., Crews, J. H., and Avva, V. S., "Modified Mixed-Mode Bending Test Apparatus for Measuring Delamination Fracture Toughness of Laminated Composites," *Journal of Composite Materials*, Vol. 32, No. 9, 1998, pp. 804–828.

[5]Salvi, A., and Waas, A. M., "Strain Rate Effects on Unidirectional Textile Carbon Fiber Composites, *Polymer Composites*, (to be published); also *ACC-EMWG Workshop Proceedings*, 2002.

[6]Caliskan, A., Automotive Composites Consortium, Energy Management Working Group, Annual Workshop Presentation, March 1999.

[7]Rosakis, A. J., Liu, C., Stout, M. G., and Coker, D., California Inst. of Technology, GALCIT SM Rept., 97-8, Pasadena, CA, Feb. 1997.

[8]Lambros, J., and Rosakis, A. J., "Shear Dominated Transonic Interfacial Crack Growth in a Bimaterial—I Experimental Observations," *Journal of the Mechanics and Physics of Solids*, Vol. 43, 1995, pp. 169–188.

[9]Liu, C., Rosakis, A. J., Ellis, R. W., and Stout, M. G., "A Study of the Fracture Behavior of Unidirectional Fiber Reinforced Composite Using Coherent Gradient Sensing (CGS) Interferometry," *International Journal of Fracture*, Vol. 90, 1998, pp. 355–369.

[10]Coker, D., and Rosakis, A., "Experimental Observations of Intersonic Crack Growth in Asymmetrically Loaded Unidirectional Composites Plates," *Philosophical Magazine A*, Vol. 81, 2001, pp. 571–595.

[11]Liu, C., Knauss, W. G., and Rosakis, A. J., "Loading Rates and the Dynamic Initiation Toughness in Brittle Solids," *International Journal of Fracture*, Vol. 90, 1998, pp. 103–118.

[12]"Standard Test Methods for Shear Properties of Composite Materials by the v-Notched Beam Method," American Society for Testing and Materials, Standard Designation: D5379/D5379M-98, 1998.

K. N. Shivakumar
Associate Editor